RSC Advances

ROYAL SOCIETY OF CHEMISTRY

PAPER

View Article Online
View Journal | View Issue

Check for updates

Cite this: *RSC Adv.*, 2022, **12**, 35300

Designing red-fluorescent superparamagnetic nanoparticles by conjugation with gold clusters

Agne Mikalauskaite,[a] Marijus Pleckaitis,[b] Giedre Grinciene,[a] Vitalijus Karabanovas[b] and Arunas Jagminas*[a]

Received 15th November 2022
Accepted 30th November 2022

DOI: 10.1039/d2ra07242d

rsc.li/rsc-advances

Photoluminescent (PL) metal and metal oxide nanoclusters (NCs), with a size of just several nanometers, are a separate class of nanomaterials abundant with new attractive optical, physical, and chemical properties and biocompatibility. However, the synthesis of PL magnetic NCs *via* attachment of PL NCs to iron oxide-based nanoparticles (NPs) is still problematic. Motivated by this, herein, we report the development of a microwave-driven conjugation approach of red-fluorescent gold nanoclusters (BSA@AuNCs) to superparamagnetic NPs. Synthesized $CoFe_2O_4$@AuNCs possess strong photoluminescence in water and ethanol media as well as good colloidal and optical stability, and magnetization response. High-resolution transmission electron microscopy (HRTEM), steady-state and time-resolved photoluminescence spectroscopy, X-ray powder diffraction (XRD), and magnetic measurements from ambient to cryogenic temperatures were applied for structural characterization and evaluation of optical and magnetic properties of the synthesized species.

Introduction

Photoluminescent metal nanoclusters consisting of several to tens of atoms, are ultra-small NPs, with size comparable with the Fermi wavelength of an electron, *ca.* $\leq$2 nm, that demonstrate intriguing physical and chemical properties.[1–5] For chemical synthesis of NCs, various ligands from phosphines[6] and thiols[7] to proteins[8–10] have been proposed. Protein-functionalized NCs of noble metals most often exhibit a strong photoluminescence signal in the visible spectral region, have high quantum yield,[11] and excellent photostability for more than one month.[12] However, upon attaching them to the surface of a magnetic NP, the red PL of AuNCs usually is completely quenched.

Superparamagnetic iron oxide-based NPs are commonly used magnetic nanocarriers for various biomedical applications, such as hyperthermia and MRI contrast agents, biosensors, biolabels, drug transporters, *etc.*[13] To prevent aggregation, they are covered with biocompatible shell of dextran, chitosan, poly(vinyl) alcohol, polyethylene oxides, proteins,[14–17] whereas to endue them with a novel surface chemistry, the subsequent attachment of desired molecules are required.[18,19] The attachment ways of Au^0 NPs to magnetic iron oxide NPs producing hybrid plasmodia nanocomposites[20–22] have been reported in several papers. Several efforts have been also made during the past decade seeking to fabricate fluorescent magnetic nanocrystals and NPs. The proposed synthesis protocols, however, required multiple steps by synchronized procedures. For example, Desmettre *et al.*[23] reported a way for fabrication of fluorescent magnetite NPs in a NIR region by covering them with copolymer shell stabilized with the azICG (azide-terminated indocyanine green) dye. However, low fluorescence quantum yield[24] and binding to proteins[25] reduced the applicability of azICG dye functionalized magnetite NPs in diagnostic technologies. Recently, dye-free luminescent magnetic NPs have been fabricated by coating with blue luminescent polymer, *ca.* branched polyethyleneimine fluorophores.[26,27] However, the fluorescence of dye molecules and quantum dots (QDs) in the visible wavelengths range usually is significantly reduced when attached to the iron oxide surface due to a strong absorption of UV and visible light. In 2018, Sony *et al.* synthesized superparamagnetic and fluorescent NPs composed of magnetite (Fe_3O_4) core and gold cluster shell by conjugation with positively charged erlotinib drug molecules. For this, arginine amino acid was attached to the surface of magnetite core *via* prolonged sonication. Red-fluorescent Au@BSA NCs, synthesized separately, were linked to the magnetite core and stabilized with erlotinib by the next processing steps.[28] However, in this case as in others, the saturation magnetization value of superparamagnetic NPs reduces after covering with fluorescent shell.

In this study, we present a new route for engineering of red-photoluminescent magnetic SPION-type NPs by conjugation with the BSA-based AuNCs. In contrast to previous reports, the synthesized magnetic NPs after conjugation with gold

---

[a] *State Research Institute Center for Physical Sciences and Technology, Sauletekio Ave. 3, LT-10254, Vilnius, Lithuania. E-mail: arunas.jagminas@ftmc.lt*

[b] *Biomedical Physics Laboratory, National Cancer Institute, LT-08406, Vilnius, Lithuania*

nanoclusters possess a higher saturation magnetization value when compared with individual ferrite NPs, and show excellent PL stability for weeks. We envisage that these NPs have prospective applications in the dual-mode diagnosis, and therapy.

Experimental

Materials

$HAuCl_4 \cdot 4H_2O$, $CoCl_2$, $FeCl_3$, PBS buffer, BSA (96%) and amino acids: D,L-cysteine (Cys, $C_3H_7NO_2S$, 96%), L-arginine (Arg, $C_6H_{14}N_4O_2$), L-lysine (Lys, $C_6H_{14}N_2O_2$), D,L-methionine (Met), and L-glutamine (Glu, $C_5H_{10}N_2O_3$, 99.5%) were purchased from Sigma-Aldrich and used without any further purification. BSA powder, was obtained from Sigma-Aldrich. Chemically pure NaOH was purchased from Posh SA, Poland and purified by over saturation of aqueous solution. Distilled water was used throughout all tests. Dialysis tubes SnakeSkin™ were purchased from Thermo Sci. (MWCO, 10 kDa, Rockford, IL, USA).

Syntheses of ferrite and magnetite NPs

Cobalt ferrite ($CoFe_2O_4$) NPs were synthesized from an alkaline aqueous solution containing 0.0275 mol L^{-1} $CoCl_2$ and 0.05 mol L^{-1} $FeCl_3$, and 0.05–0.2 mol L^{-1} of amino acid as chelating agent. NaOH aqueous solution was used to adjust the pH of solution to 12.2. The syntheses were conducted in the Teflon line autoclave at 130 °C for up to 10 h. The products were collected by centrifugation and magnetic collection, then rinsed and dried at 60 °C overnight.

Synthesis of luminescent Co ferrite NPs

The following procedure has been designed for formation of red-photoluminescent magnetic nanoparticles. Briefly, 100 µg of $CoFe_2O_4$ NPs were added to 5 mL 2-(*N*-morpholino)ethanesulfonic acid buffer (MES) at a pH 6.3 and sonicated for 30 min. In other glass, 0.25 g of bovine serum albumin (BSA) were dissolved in aqueous 5 mL of $HAuCl_4$ (10 mmol L^{-1}) solution. Subsequently, both solutions were mixed, and pH adjusted to 12.4 by dropwise addition of 1 mol L^{-1} NaOH solution. The obtained solution was transferred to a 35 mL microwave vial and quickly heated by microwave radiation (160 W) at 60 °C for 1 h. After reaction, the solution was cooled down naturally to room temperature. Obtained products were collected by centrifugation and washed with deionized water. Ultrasmall NPs were collected using a permanent magnet. Up to five experiments were carried out to account for data discrepancy. The purification of NP solutions was performed by dialysis against distilled water for 12 h using a dialysis membrane SnakeSkin™.

Characterization

The morphology of as-synthesized NPs was studied by TEM FEI Tecnai F20X-TWIN, operated at an accelerating voltage of 200 kV. The NPs subjected to observations were dispersed in EtOH on a carbon-coated Ni grid. The size distribution histograms of NPs were estimated using the ImageJ software. Phase analysis of ferrite NPs was analyzed using X-ray powder D8 diffractometer (Bruker AXC, Germany) equipped with a Göbel mirror with rotating Cu anode as a primary beam monochromator for CuK_α radiation in the range from 10° to 75° with a step size 0.02° and a counting time 8 s per step. Phase identifications were performed using database PDF4+ and the size of crystallites was estimated by the Halder–Wagner (H–W) approximation. UV-vis absorption spectra were recorded using a Shimadzu 2450 spectrometer and the photoluminescence spectra were recorded on an Edinburgh F900 fluorescence spectrometer (Edinburgh instruments Ltd, UK) equipped with a picosecond pulsed diode laser EPL-470 employed for excitation of samples at $\lambda_{ex} = 470$ nm and $\lambda_{ex} = 375$ nm.

Fluorescence decay measurements were acquired by a time-correlated single-photon counting technique using FLS 920 spectrometer (Edinburgh instruments Ltd) equipped with a single photon photomultiplier detector (S900-R) (Hamamatsu, Japan) and diode laser ($\lambda = 405$ nm, pulse length – <200 ps, pulse repetition rate – 200 kHz) for excitation of

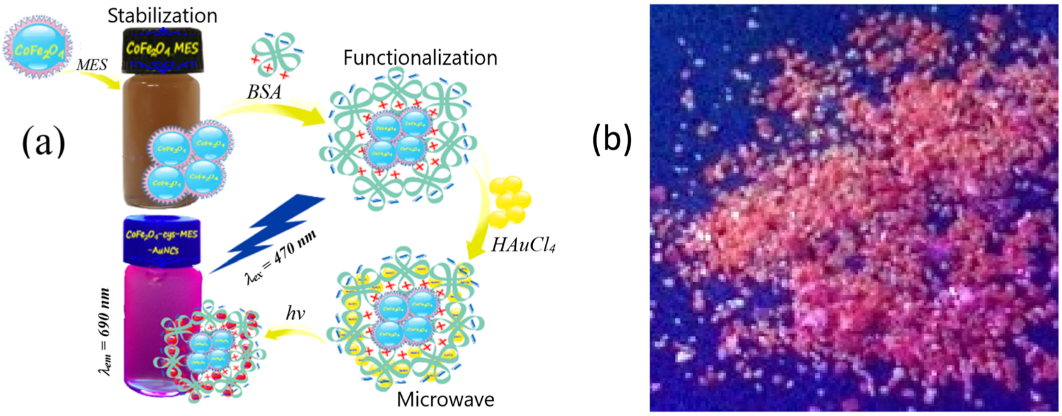

Fig. 1 (a) Schematic representation of the synthesis route of amino acid-stabilized magnetic nanoparticles followed by their microwave-assisted conjugation with amino acid and protein driven Au nanoclusters. (b) The typical photo of red-fluorescent synthesized products under $\lambda_{ex} = 375$ nm.

$CoFe_2O_4$@AuNC and Fe_3O_4@AuNC solutions in PBS. Photoluminescence decay was measured by collecting 1000 counts at the peak emission wavelength (~700 nm) of the $CoFe_2O_4$@AuNCs PL band. Average fluorescence lifetime was calculated using eqn (1):

$$\langle \tau_{\mathrm{ave}} \rangle = \frac{B_1\tau_1^{\,2} + B_2\tau_2^{\,2} + B_3\tau_3^{\,2}}{B_1\tau_1 + B_2\tau_2 + B_3\tau_3} \tag{1}$$

where B_1 is the amplitude of the first exponential term, B_2 is that of the second term, and so forth and τ_1 is the PL lifetime of the first exponential term, τ_2 is that of the second term, and so forth.

The quantum yield (QY) of photoluminescent NPs formation inside microwave reactor was calculated by comparing the PL intensities of the sample to that of a standard fluorescent dye, PD17, in ethanol with QY 97–99%. Magnetization measurements were accomplished *versus* applied magnetic field at 4 K to 300 K temperature using a vibrating sample magnetometer calibrated by a Ni sample.

Results and discussion

Fig. 1 depicts the synthesis scheme of magnetic-fluorescent nanoparticles designed in this study. As reported in the Experimental section, two-step synthesis was used for fabrication of ultrasmall cobalt ferrite NPs stabilized with amino acid and the subsequent their conjugation with BSA driven red-luminescent gold nanoclusters. The XRD pattern of hydrothermally synthesized Co ferrite NPs from an alkaline Co(II) and Fe(III) chloride solutions with cysteine amino acid, implied formation of $CoFe_2O_4$ containing crystalline NaCl as side phase (Fig. 2a).

Closer inspection of this XRD spectrum within 2Θ range from 10° to 75° reveals the presence of all main diffraction peaks at 30.08°, 35.44°, 43.06°, and 62.58°, characteristic to $CoFe_2O_4$ planes (220), (311), (400), and (440), respectively, listed in the DB card no. 01-083-4766. The inclusion of crystalline NaCl species in the as-grown ferrite species is clearly seen from the diffraction peaks at 2Θ angles 31.70°, 45.45°, and 56.47° positions (Fig. 2a, plot 1), corresponding to the planes of NaCl (200), (220), and (222), respectively (DB card no. 01-085-8594). Note that upon rinsing in water pure $CoFe_2O_4$ product was obtained (Fig. 2a, pattern 2).

The attaching of gold to $CoFe_2O_4$ species upon the subsequent processing in the microwave reactor was also verified by XRD pattern depicted in Fig. 2a (plot 3) since the typical diffraction peaks from the main gold planes (111), (200), and (220) at 2Θ angles 38.18°, 44.39°, and 64.58°, respectively, are viewed (DB card no. 00-004-0784).

The formation and attachment of gold nanoclusters to $CoFe_2O_4$ NPs was verified further by photoluminescence measurements of as-synthesized and dialyzed $CoFe_2O_4$@AuNCs NPs (Fig. 2b). From the HRTEM observations (Fig. 3a), the average size of as-formed $CoFe_2O_4$ NPs stabilized with D,L-cysteine under the adapted herein hydrothermal synthesis conditions is about 2.4 nm (Fig. 3a). The dialysis of photoluminescent $CoFe_2O_4$@AuNCs species resulted in the enhancement of PL and blue shift of PL peak from 700 nm to 680 nm (Fig. 2b) most likely due to the decrease in size, which is typical for gold nanoclusters. It was, however, determined that using subsequent microwave-assisted treatment to conjugate ferrite NPs with Au@BSA nanoclusters, resulted in tenfold increase in the nanoprobes size (Fig. 3b). It was established that fluorescence intensity and stability of NPs depended on the concentration of $CoFe_2O_4$–Cys NPs inserted in the microwave synthesis reactor (Fig. 4). Under blue light excitation, the synthesized hybrid-type NPs emitted at around 700 ± 10 nm, which is quite similar to the PL of pure Au@BSA nanoclusters (Fig. 5a).[8] Based on the spherical Jellium model,[29] we can suspect the presence of Au27–Au29 clusters entrapped inside the hybrid particle. The PL spectra presented in Fig. 5, show that PL of the BSA gold nanocluster solutions synthesized together with Co ferrite NPs is almost 6 times weaker than Au@BSA nanoclusters alone (Fig. 5a, spectra 1 and 3). We determined here that the addition of amino acids to the synthesis solution of hybrid species can enhance (lysine, glutamine) or not

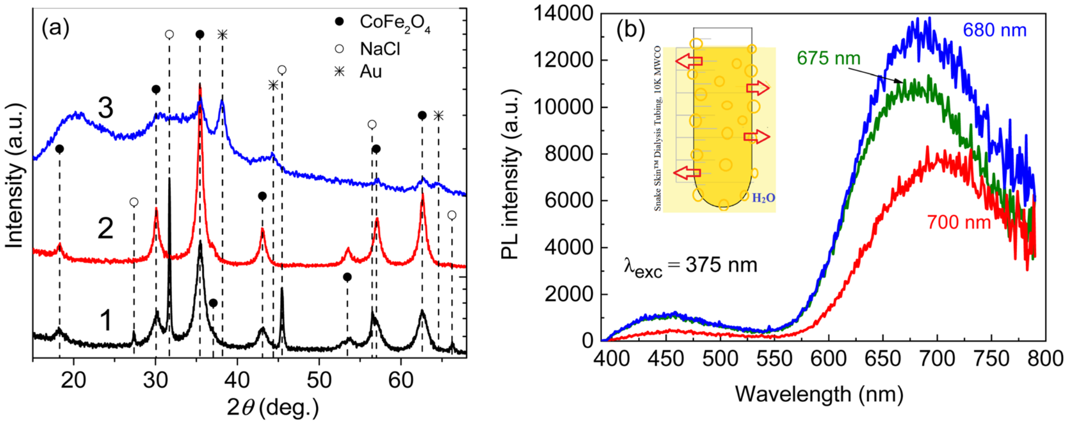

Fig. 2 (a) XRD patterns of NPs synthesized hydrothermally in a solution containing $0.0275CoCl_2 + 0.05FeCl_3 + 0.05\ \mathrm{mol\ L^{-1}}$ Cys + NaOH to pH = 12.15 at 130 °C for 10 h before (1), after rinse (2), and gold cluster attachment (3). (b) The photoluminescence spectra of the same rinsed $CoFe_2O_4$ NPs conjugated with BSA-driven gold NCs after dialysis for 12 (red), 24 (green) and 48 h (blue). $\lambda_{ex} = 375$ nm. In the inset, the dialysis scheme.

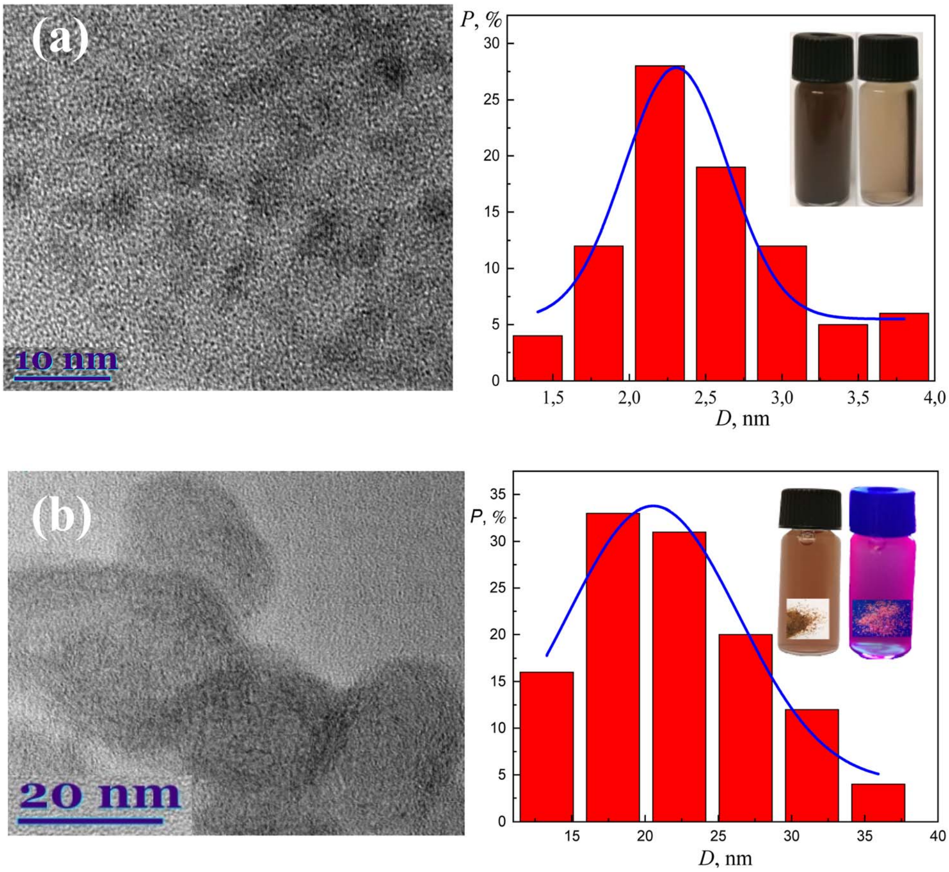

Fig. 3 HRTEM images of $CoFe_2O_4$–Cys NPs (a) and $CoFe_2O$–Cys@AuNCs NPs (b) and their corresponding size distribution histograms (right panels). $\lambda_{ex} = 375$ nm. In the insets: the color of the corresponding nanoprobes under vis. and UV (the bottles on the in right) illuminations.

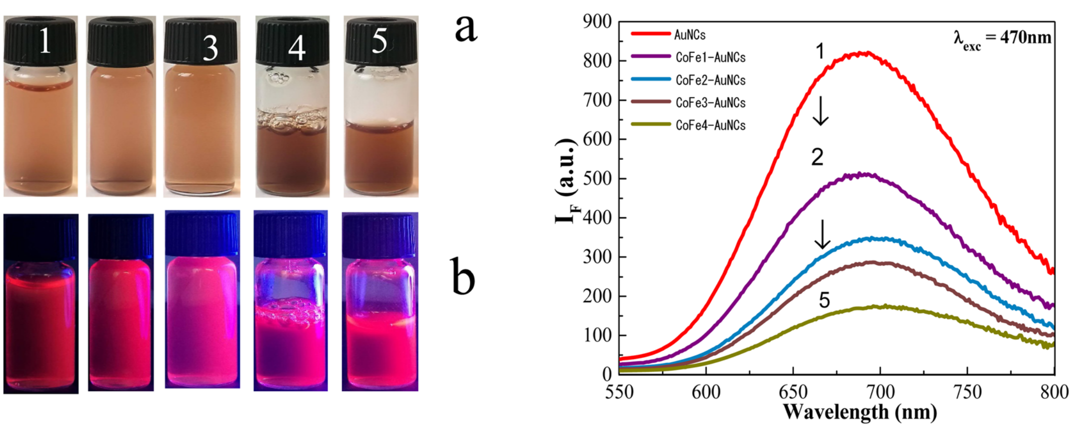

Fig. 4 The photo of $CoFe_2O_4$@AuNCs NP solutions before (a) and after (b) excitation with blue light (470 nm) on the concentration of $CoFe_2O_4$@Cys NPs in the synthesis solution: 1–0, 2–2.43, 3–7.28, 4–21.83, and 5–29.13 mg mL^{-1}. On the right side: PL spectra of the corresponding hybrid NPs. The synthesis and attachment of gold clusters to $CoFe_2O_4$ was performed by microwave processing at 60 °C for 1 h.

influence (arginine) PL intensity (Fig. 5b). The reasons for such influence are not clear and will be studied in a separate study.

Noteworthy that after leaving solutions for three weeks in water or PBS buffer at 4 °C, hybrid $CoFe_2O_4$ NPs preserved fluorescent properties. Moreover, the conjugated Au@BSA clusters to Co ferrite NPs remained fluorescent after two–three weeks, even in 5–6% intense compared to as-formed ones.

Time-resolved fluorescence spectroscopy measurements were made using 405 nm pulsed diode laser and are presented in Fig. 6a. Decay of photoluminescence at ~700 nm was fitted with the tri-exponential tail-fitting model.[30] A fast exponential

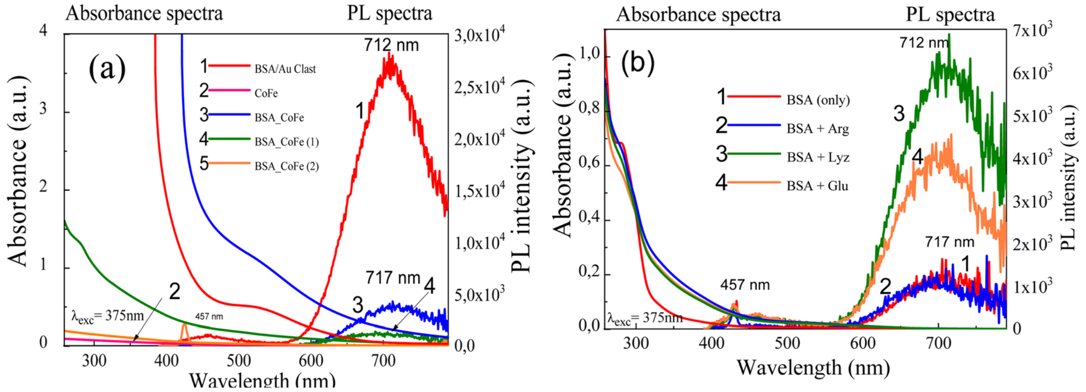

Fig. 5 Absorbance and photoluminescence spectra of gold cluster solutions prepared from BSA + $HAuCl_4$ + NaOH to pH = 12.4 at 60 °C for 1 h without (1) and containing tabulated $CoFe_2O_4$ NPs (a) or indicated amino acids (b): arginine (2), lysine (3), glutamine (4).

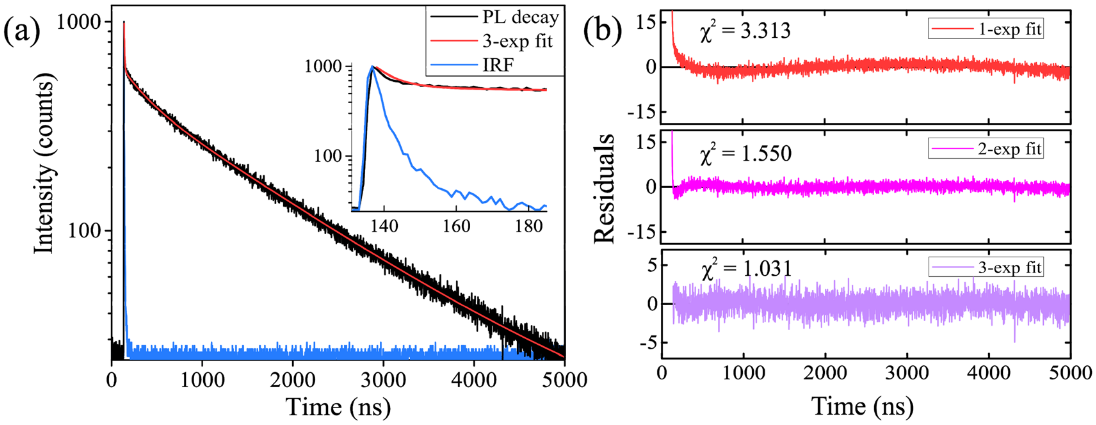

Fig. 6 Photoluminescence decay curve of $CoFe_2O_4$@AuNCs after preparation in PBS (black decay) and its tri-exponential fit (red line) (a). Inset represents a zoomed region from 130 ns to 185 ns. Light blue decay shows instrument response function (IRF). Quality of the mono-, bi-, and tri-exponential tail-fits represented by residuals and χ^2 (b).

component (τ_1) was in the range of ~5.8 ns and could be attributed to the instrument response function. An intermediate component (τ_2) had a lifetime of ~268 ns and a long-lifetime component (τ_3) was ~1495 ns.

They resulted in an average PL lifetime of ~1423 ns. Mono- and bi-exponential tail-fitting models were inaccurate, and the best fit for $CoFe_2O_4$@AuNCs in PBS was achieved with the tri-exponential model. Quality of the fits is represented by residuals and χ^2, which were 3.313, 1.550, and 1.031 for mono-, bi-, and tri-exponential fits, respectively (Fig. 6b). In our previous studies, we demonstrated that BSA[31] or human blood plasma protein-stabilized[32] gold nanoclusters alone had similar optical properties as do herein reported $CoFe_2O_4$@AuNCs. Yang *et al.* showed that noble metal nanoclusters exhibit metal-centered and ligand-centered emissions, which could be attributed to the shorter PL lifetimes in the range of nanoseconds and longer lifetimes in the range of microseconds, respectively.[33] This could explain the bi-exponential nature of $CoFe_2O_4$@AuNCs photoluminescence. Long-lived excited state of Au NCs photoluminescence creates highly favorable conditions for the generation of various reactive oxygen species, making it possible to use gold nanoclusters as photosensitizers for photodynamic therapy.[31,33]

The zeta-potential (ξ) of hydrothermally synthesized Au@BSA nanoclusters (≅−16.6 eV), as well as $CoFe_2O_4$–Cys NPs, hybridized with these NCs was found to be negative. The magnitude of ξ-potential measured for hybrid NPs is larger than that of entrapped Au@BSA nanoclusters. From the experimental results (Table 1), the ξ-potential value of hybrid NPs

Table 1 Variables of zeta-potential on the concentration of $CoFe_2O_4$@AuNC NPs in MES solution

No.	NP	Conc. (mg mL^{-1})	ζ (eV)
0	Au_{NC} sol.	0	−16.6
1	$CoFe_2O_4$@AuNC	2.43	−18.6
2	$CoFe_2O_4$@AuNC	7.28	−25.7
3	$CoFe_2O_4$@AuNC	10.52	−26.3
3	$CoFe_2O_4$@AuNC	14.56	−25.5
4	$CoFe_2O_4$@AuNC	21.83	−23.5
5	$CoFe_2O_4$@AuNC	29.13	−22.0
6	$CoFe_2O_4$@AuNC	38.82	−28.1

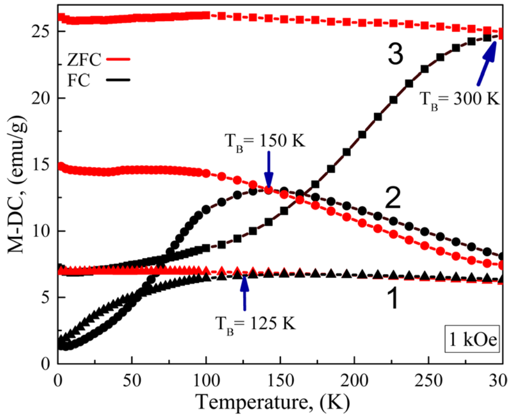

Fig. 7 Temperature-dependent magnetization curves for zero-field-cooled (ZFC) and 1 kOe field-cooled (FC) ultrasmall $CoFe_2O_4$ NPs (1), 2.4 nm-sized $CoFe_2O_4$ NPs (2), and (3) Au@BSA nanoclusters-coated 2.4 nm-sized $CoFe_2O_4$ NPs at the indicated temperatures.

depends on the amount of ferrite NPs added to the microwave reactor to synthesize fluorescent NPs. Consequently, the ξ-potential of hybridized NPs designed from 2.4 nm-sized $CoFe_2O_4$–Cys NPs and BSA-driven gold nanoclusters vary with the entrapped amount of $CoFe_2O_4$–Cys NPs increasing to $\cong -26$ eV for probes containing 10–15 mg mL^{-1} of ferrite (Table 1). Further increase in the concentration of ferrite NPs just slightly influenced their ξ-potential after hybridization. However, the aqueous solutions containing more than 20 mg mL^{-1} of NPs tend to agglomerate (see samples no 4 and no 5 in Fig. 4). Noticing, the highest ξ-potential values should be ascribed to the most stable NPs.

Magnetic properties of as-synthesized ultrasmall (remained in the synthesis solution after centrifugation) and 2.4 nm-sized $CoFe_2O_4$–Cys NPs before and after hybridization with gold NCs were studied in the temperature range from 300 K to 4 K under zero-field-cooling (ZFC) and field cooling (FC) conditions at an applied field of 1 kOe. Fig. 7 shows the ZFC/FC curves and superparamagnetic blocking temperature (T_B) increase from 125 K to 300 K, clearly identifying by the peak positions at the ZFC branch for ultrasmall (125 K) and 2.4 nm-sized (150 K), and hybrid (fluorescent) (300 K) NPs, respectively. T_B increase we ascribed to the size increase of analyzed NPs as in ref. 30.

The magnetic hysteresis curves obtained for 2.4 nm-sized cobalt ferrite NPs synthesized in this study with cysteine before and after hybridization with Au@BSA nanoclusters at various temperatures are depicted in Fig. 8. From these, all samples have open hysteresis at $T = 4$ K, while at $T = 200$ K only ensembled NPs preserve their hysteretic behavior. At ambient temperature ($T = 300$ K), however, all NPs become superparamagnetic in accordance with the ZFC/FC curves in Fig. 7. Moreover, the MS value of ferrite NPs increased after conjugation with Au@BSA nanoclusters to 42.58 emu g^{-1} at $T = 300$ K. Therefore, it can be concluded that the best superparamagnetic behavior and stability possessed Au@BSA entrapped 2.4 nm-sized $CoFe_2O_4$–Cys NPs, which saturation magnetization value approximated to 34.9 emu g^{-1}. Note that a slow M_S increase to saturation value characteristic for ferrite NPs before hybridization at $T = 300$ K (Fig. 8c) compared to $M_S(H)$ plots run at other

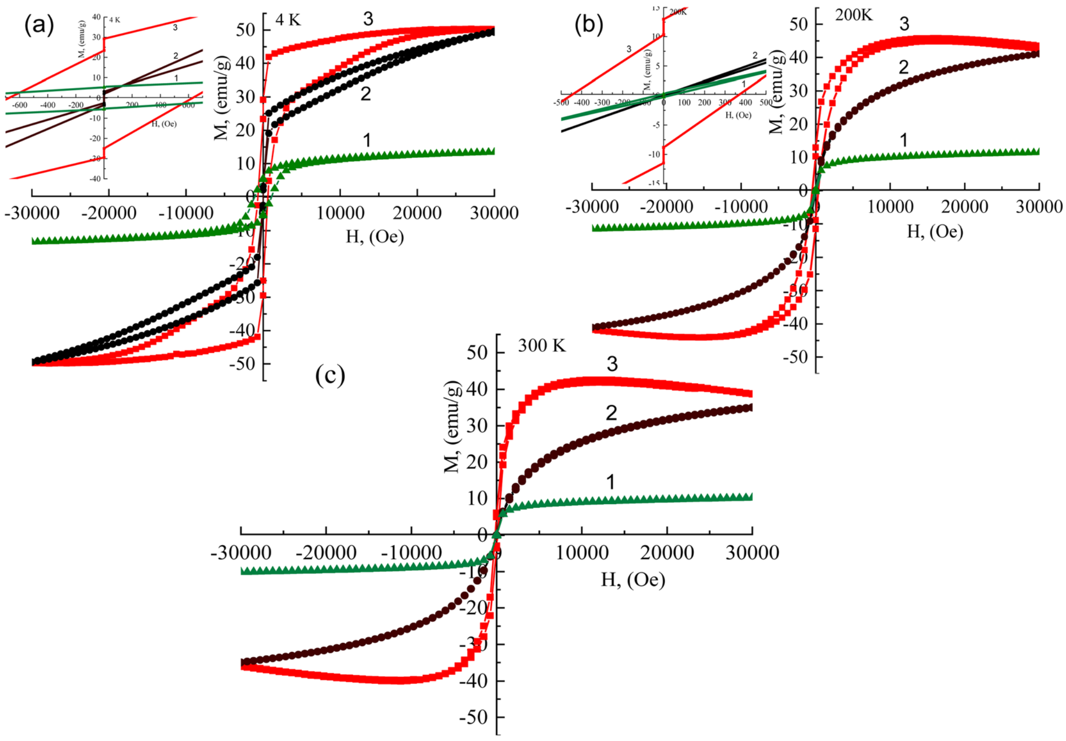

Fig. 8 Hysteresis loops, $M(H)$, at 4 K (a), 200 K (b), and 300 K (c) temperatures of ultrasmall $CoFe_2O_4$ (1), 2.4 nm-sized $CoFe_2O_4$–Cys (2) and Au@BSA NCs-coated 2.4 nm-sized $CoFe_2O_4$–Cys NPs (3), respectively.

Table 2 Magnetic characteristics of as-synthesized with cysteine $CoFe_2O_4$ NPs before and after hybridization with Au@BSA nanoclusters. Saturation magnetization, M_S, blocking temperature, T_B, coercive field, H_C, and remanent magnetization, M_R

	M_S (emu g^{-1})				H_C (Oe)		M_R (emu g^{-1})		
Samples	4 K	200 K	300 K	T_B (K)	200 K	4 K	4 K	200 K	300 K
Ultrasmall $CoFe_2O_4$ NPs	13.44	11.48	10.17	125	—	—	—	—	—
2.4 nm-sized $CoFe_2O_4$ NPs	49.6	41.1	34.9	150	—	—	—	—	—
Au@BSA CLs-coated NPs	50.32	45.82	42.58	300	800	1200	30	10	—

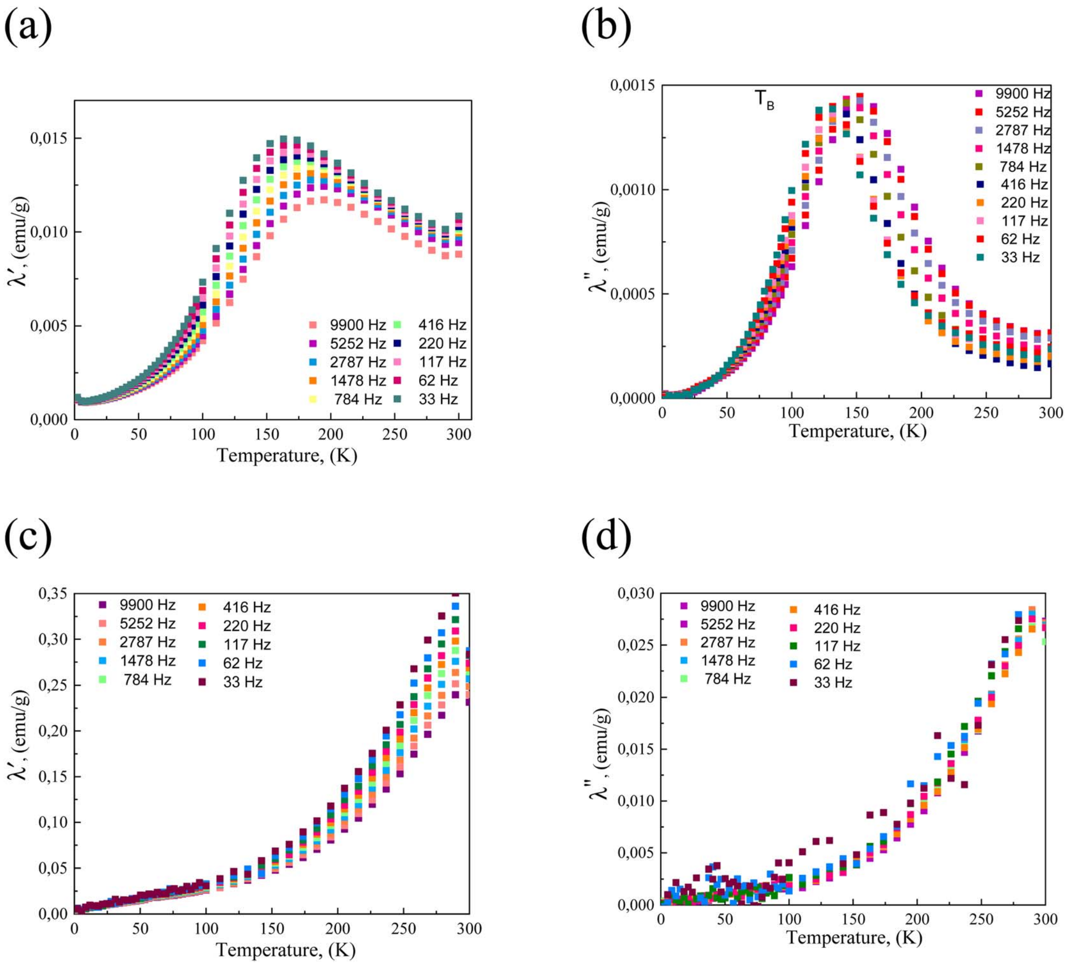

Fig. 9 Magnetic susceptibility *vs.* temperature at the indicated ac frequencies for 2.4 nm-sized $CoFe_2O_4$ (a and c) NPs before (a) and after conjugation with gold clusters (c). (b and d) The T_B plots at indicated frequencies for the same nanoparticles.

temperatures also implied the good magnetic properties of this sample. The presence of a loop for hybrid NPs at 4 K, its decrease at 200 K, and its disappearance at ambient temperatures we linked to the core spins coupled with the frozen disordered surface spins.[34] Despite the spherical structure of gold clusters entrapped with 2.4 nm-sized $CoFe_2O_4$–Cys NPs in tenfold larger ensembles, their reduced remanent M_R/M_S values at 4 K and 200 K equaled to 0.59 and 0.22, respectively, which at 4 K is close to the theoretical value of 0.5 expected for no interacting uniaxial single-domain particles with the easy axis randomly oriented.[35] The saturated magnetization, M_S, blocking temperature, T_B, coercive field, H_C, and remanent magnetization, M_R, values for investigated herein magnetic Co ferrite NPs are presented in Table 2.

The temperature-dependent magnetic susceptibility plots for ultrasmall, 2.4 nm-sized $CoFe_2O_4$–Cys and hybrid-type $CoFe_2O_4$–Au@BSA_{NCs} NPs at various external alternating current (ac) magnetic field frequencies within 33 Hz to 9.9 kHz range are shown in Fig. 9. As seen, the magnetic susceptibility of the 2.4 nm-sized $CoFe_2O_4$–Cys NPs initially increases and reaches a maximum value in a vicinity of the blocking temperature at about 150–175 K. For these NPs above the T_B, the susceptibility (χ) follows the modified Curie-law: $\chi = \chi_0 + C/T$. The shapes of temperature-dependent susceptibility plots for the same Co ferrite NPs after conjugation with gold NCs change significantly (Fig. 9c and d), indicating T_B increase to 300 K and higher most likely due to the hybrid NPs size increase compatible with TEM observations (Fig. 3b).

Conclusions

We developed the conjugation way of superparamagnetic cobalt ferrite NPs with red-photoluminescent gold nanoclusters by microwave-assisted treatment. From the TEM observations, zeta-potentials, and magnetic measurements of the synthesized hybrid-type NPs, we concluded that they are composed of several 2.4 nm-sized $CoFe_2O_4$ NPs and gold nanoclusters forming tenfold larger assembles with high stability as well as enhanced magnetic and fluorescent properties. The novel red-photoluminescent superparamagnetic NPs with an average lifetime of about 1.4 μs could play a pivotal role in early disease diagnostics and molecular bioimaging.

Author contributions

A. J. conceived this study and wrote the manuscript. A. M., M. P., and G. G. performed the experiments, V. K. critically reviewed and edited the manuscript. All authors have read and approved the final manuscript.

Conflicts of interest

The authors indicate there are no conflicts to declare.

Acknowledgements

Dr Agne Mikalauskaite acknowledges a fellowship from the Research Council of Lithuania and the Ministry of Foreign Affairs and International Cooperation.

References

1 H. T. Sun and Y. Sakka, Luminescent metal nanoclusters: controlled synthesis and functional applications, *Sci. Technol. Adv. Mater.*, 2014, **15**, 014205.
2 P. L. Xavier, K. Chaudhari, P. K. Verma, S. K. Pal and T. Pradeep, Luminescent quantum clusters of gold in transferrin family protein, lactoferrin exhibiting FRET, *Nanoscale*, 2010, **2**, 2769–2776.
3 R. C. Jin, Quantum sized, thiolate-protected gold nanoclusters, *Nanoscale*, 2010, **2**, 343–362.
4 L. Shang, S. J. Dong and G. U. Nienhaus, Ultra-small fluorescent metal nanoclusters: synthesis and biological applications, *Nano Today*, 2011, **6**, 401–418.
5 S. Choi, R. M. Dickson and J. H. Yu, Developing luminescent silver nanodots for biological applications, *Chem. Soc. Rev.*, 2012, **41**, 1867–1891.
6 M. Osawa, M. Hoshino, M. Akita and T. Wada, Synthesis and characterization of phenanthryl-phosphine gold complex: observation of room temperature, *Inorg. Chem.*, 2005, **44**, 1157–1159.
7 A. C. Templeton, W. P. Wuelfing and R. W. Murray, Monolayer protected cluster molecules, *Acc. Chem. Res.*, 2000, **33**, 27–36.
8 J. Xie, Y. Zheng and J. Y. Ying, Protein-directed synthesis of highly fluorescent gold nanoclusters, *J. Am. Chem. Soc.*, 2009, **131**, 888–889.
9 M. B. Dickerson, K. H. Sandhage and R. R. Naik, Protein- and peptide-directed syntheses of inorganic materials, *Chem. Rev.*, 2008, **108**, 4935–4978.
10 X. L. Guevel, N. Daum and N. M. Schneider, Synthesis and characterization of human transferrin stabilized gold nanoclusters, *Nanotechnology*, 2011, **22**, 275103.
11 I. Nandi, S. Chall, S. Chowdhury, T. Mitra, S. S. Roy and K. Chattopadhyay, Protein fibril-templated biomimetic synthesis of highly fluorescent gold nanoclusters and their applications in cysteine sensing, *ACS Omega*, 2018, **3**, 7703–7714.
12 A. K. Gupta and M. Gupta, Synthesis and surface engineering of iron oxide nanoparticles for biomedical applications, *Biomaterials*, 2005, **26**, 3995–4021.
13 W. H. Suh, K. S. Suslick, G. D. Stucky and Y. H. Suh, Nanotechnology, nanotoxicology, and neuroscience, *Prog. Neurobiol.*, 2009, **87**, 133–170.
14 X. Zhao and J. M. Harris, *J. Pharm. Sci.*, 1998, **87**, 1450–1458.
15 R. Hao, R. J. Xing, Z. C. Xu, Y. L. Hou, S. Gao and S. H. Sun, Synthesis, functionalization, and biomedical applications of multifunctional magnetic nanoparticles, *Adv. Mater.*, 2010, **22**, 2729–2742.
16 M. Anbarasu, M. Anandan, E. Chinnasamy, V. Gopinath and K. Balamurugan, Synthesis and characterization of polyethylene glycol (PEG) coated Fe_3O_4 nanoparticles by chemical co-precipitation method for biomedical applications, *Spectrochim. Acta, Part A*, 2015, **135**, 536–539.
17 S. A. Corr, Y. P. Rakovich and Y. K. Guriko, Multifunctional Magnetic Fluorescent Nanocomposites for Biological Applications, *Nanoscale Res. Lett.*, 2008, **3**, 87–104.
18 R. D. Rutledge, C. L. Warner, J. W. Pittman, R. S. Addleman, M. Engelhard, W. Chouyyok and M. G. Warner, Thiol-Ene Induced Diphosphonic Acid Functionalization of Superparamagnetic Iron Oxide Nanoparticles, *Langmuir*, 2010, **26**, 12285–12292.
19 J. L. Lyon, D. A. Fleming, M. B. Stone, P. Schiffer and M. E. Williams, Synthesis of Fe oxide core/Au shell nanoparticles by iterative hydroxylamine seeding, *Nano Lett.*, 2004, **4**, 719–723.
20 T. A. Larson, J. Bankson, J. Aaron and K. Sokolov, Hybrid plasmonic magnetic nanoparticles as molecular specific agents for MRI/optical imaging and photothermal therapy of cancer cells, *Nanotechnology*, 2007, **18**, 325101.
21 A. Mikalauskaitė, R. Kondrotas, G. Niaura and A. Jagminas, Gold-Coated Cobalt Ferrite Nanoparticles via Methionine Induced Reduction, *J. Phys. Chem. C*, 2015, **119**(30), 17398–17407.
22 M. D. Daniele, L. M. Shoughnessy, R. Roeder, A. Childress, Y. P. Bandera and S. Foulger, Magnetic Nanoclusters

Exhibiting Protein-Activated Near Infrared Fluorescence, *ACS Nano*, 2013, **7**(1), 203–213.

23 T. Desmettre, J. M. Devoisselle and S. Mordon, Fluorescence properties and metabolic features of indocyanine green (ICG) as related to angiography, *Surv. Ophthalmol.*, 2000, **45**, 15–27.

24 R. Simmons and R. J. Shephard, Does indocyanine green obey Beer's law?, *J. Appl. Physiol.*, 1971, **30**, 502–507.

25 T. J. Muckle, Plasma proteins binding of indocyanine green, *Biochem. Med.*, 1976, **15**, 17–21.

26 R. Khodadust, O. Unal and H. Y. Acar, Theranostic potential of self-luminescent branched polyethyleneimine-coated superparamagnetic iron oxide nanoparticles, *Beilstein J. Nanotechnol.*, 2022, **13**, 82–95.

27 R. Kas, E. Sevinc, U. Topan and H. Y. Acar, A universal method for the preparation of magnetic and luminescent hybrid nanoparticles, *J. Phys. Chem. C*, 2010, **114**, 7758–7766.

28 J. Nebu, J. S. Anjali Devi, R. S. Aparna, K. Abha and G. Sony, Erlotinib conjugated gold nanoclusters enveloped magnetic iron oxide nanoparticles – a targeted probe for imaging pancreatic cancer cells, *Sens. Actuators*, 2018, **257**, 1035–1043.

29 J. Zheng, C. W. Zhang and R. M. Dickson, Highly fluorescent, water soluble, size-tunable gold quantum dots, *Phys. Rev. Lett.*, 2004, **93**, 077402.

30 C. Liu, A. J. Rondinone and Z. J. Zhang, Synthesis of magnetic spinel ferrite $CoFe_2O_4$ nanoparticles from ferrite salt and characterization of the size-dependent superparamagnetic properties, *Pure Appl. Chem.*, 2000, **72**, 37–45.

31 V. Poderys, G. Jarockyte, S. Bagdonas, V. Karabanovas and R. Rotomskis, Protein-stabilized gold nanoclusters for PDT: ROS and singlet oxygen generation, *J. Photochem. Photobiol., B*, 2020, **204**, 111802.

32 G. Jarockyte, V. Poderys, V. Barzda, V. Karabanovas and R. Rotomskis, Blood plasma stabilized gold nanoclusters for personalized tumor theranostics, *Cancers*, 2022, **14**(8), 1887.

33 T. Yang, S. Dai, H. Tan, Y. Zong, Y. Liu, K. Zhang, P. Wu, S. Zhang, J. Xu and Y. Tian, Mechanism of Photoluminescence in Ag Nanoclusters: Metal-Centered Emission versus Synergistic Effect in Ligand-Centered Emission, *J. Phys. Chem. C*, 2019, **123**(30), 18638–18645.

34 M. Muroi, R. Street, P. G. McCormick and J. Amighian, *Phys. Rev. B: Condens. Matter Mater. Phys.*, 2001, **63**, 184414.

35 E. C. Stoner and E. P. Wohlfart, *Philos. Trans. R. Soc. London, Ser. A*, 1948, **240**, 599–607.